Geophysical Research Letters

Key Points:
- Satellite-derived bathymetry using passive sensors, requires elevation "seed points" to yield physically meaningful seafloor elevations.
- NASA ICESat-2 laser altimetry provides a vertical reference for satellite-derived bathymetry products.
- Operationally efficient ICESat-2-aided satellite-derived bathymetry workflows hold promise for global assessment of benthic habitat change.

Correspondence to:
L. A. Magruder,
magruder@arlut.utexas.edu

ICESat-2 Elevation Retrievals in Support of Satellite-Derived Bathymetry for Global Science Applications

Benjamin J. Babbel[1], Christopher E. Parrish[1] , and Lori A. Magruder[2,3]

[1]Department of Civil and Construction Engineering, Oregon State University, Corvallis, OR, USA, [2]Applied Research Laboratories, University of Texas at Austin, Austin, TX, USA, [3]Department of Aerospace Engineering and Engineering Mechanics, University of Texas at Austin, Austin, TX, USA

Abstract Bathymetry retrievals from 2D, multispectral imagery, referred to as Satellite-Derived Bathymetry (SDB), afford the potential to obtain global, nearshore bathymetric data in optically clear waters. However, accurate SDB depth retrievals are limited in the absence of "seed depths." The Ice, Cloud, and land Elevation Satellite-2 (ICESat-2) space-based altimeter has proven capable of accurate bathymetry, but methods of employing ICESat-2 bathymetry for SDB retrievals over broad spatial extents are immature. This research aims to establish and test a baseline methodology for generating bathymetric surface models using SDB with ICESat-2. The workflow is operationally efficient (17–37 min processing time) and capable of producing bathymetry of sufficient vertical accuracy for many coastal science applications, with RMSEs of 0.96 and 1.54 m when using Sentinel-2 and Landsat 8, respectively. The highest priorities for further automation have also been identified, supporting the long-range goal of global coral reef habitat change analysis using ICESat-2-aided SDB.

Plain Language Summary Mapping the underwater surface in coastal areas is important for understanding our changing climate and how it impacts the nearshore environment. Space-based imagers are critical to underwater mapping, given their global coverage and wide spatial extent, but require reference depth measurements to inform accurate bathymetric retrievals. Laser altimetry from ICESat-2 has the potential to address the reference measurement need. This work establishes a foundational technical approach for combining the data and producing a nearshore bathymetric product that is efficient, accurate and informs new research opportunities.

1. Introduction

Nearshore bathymetry continues to be an active area of study, based on its significant contribution to coastal dynamics analysis and prediction while providing a foundation for benthic science. However, the data are difficult to acquire, since local methods are spatially limited and satellite-based methods based on spectral data generally only provide relative depth estimates that must be calibrated using independent, discrete "ground truth," or "seed" depths. These seed depths are typically provided by airborne bathymetric lidar or boat-based sonar (e.g., multibeam echosounders), which are locally constrained techniques. The conflation and fusion of passive satellite observations with active sensor measurements or in situ data creates satellite-derived bathymetry (SDB). Most SDB algorithms make use of the wavelength-dependent attenuation of downwelling irradiance with depth for different spectral bands within the visible portion of the electromagnetic spectrum (Jerlov, 1976), as modeled by the Beer-Lambert law. One widely used method, developed by Stumpf et al. (2003), estimates depths from ratios of logarithms of image values in two spectral bands, typically, blue and green, in which transmittance tends to be greater than in longer-wavelength bands in most water types. By regressing the seed depths on the relative ratio-of-logarithms bathymetry estimates, the parameters of a linear transformation from relative bathymetry to absolute bathymetry (relative to the same vertical datum as the seed depths) are obtained. While it is generally accepted that bathymetry estimation techniques based on passive remote sensing are less accurate than those that utilize active remote sensing technology (Mavraeidopoulos et al., 2017), SDB can still provide meaningful results for a variety of applications. Examples of these applications include improvements to coastal management parameters, mapping benthic habitats, coastal navigation, and conservation strategies (Eugenio et al., 2015; Pe'eri et al., 2016; Poursanidis et al., 2019).

NASA's Ice, Cloud, and Land Elevation Satellite-2 (ICESat-2) launched in September 2018. ICESat-2 carries a single instrument, ATLAS (Advanced Topographic Laser Altimeter System). ATLAS is a six-beam, high-repetition rate (10 kHz), photon-counting, green (532 nm) Earth observing lidar (Magruder et al., 2019; Markus et al., 2017). The beams are configured into three beam pairs, each separated by 3.3 km in the across-track direction with a 90 m across-track separation within the pair components. The across-track spacings are designed to decouple local surface slope from elevation change in the case of repeat measurements. At an average altitude of 496 km the instrument produces an 11 m footprint, with an along-track spot spacing of 0.7 m (center to center) for each beam (Magruder et al., 2020).

The ICESat-2 mission is dedicated to global laser altimetry with a focus on cryospheric observations to determine elevation changes in our ice sheets and capture sea ice characterization for both the Arctic and Antarctic regions. All of these data will provide a window into our planet's climate dynamics as changes in the polar regions are often the most revealing response to the Earth's processes that rely on atmospheric and thermal influences (Markus et al., 2017). Since the primary scientific goals of ICESat-2 are focused on cryospheric science with secondary objectives for vegetation mapping and atmospheric studies, there was not a dedicated approach developed prelaunch to achieve bathymetric retrievals for benthic science. However, early ICESat-2 prelaunch studies using high-altitude prototype ATLAS observations first identified the potential for identifying inland and nearshore bathymetry (Forfinski-Sarkozi & Parrish, 2016; Jasinski et al., 2016). Subsequently, initial on-orbit data analysis revealed ICESat-2's capability to provide potential seed elevation data for SDB (Albright & Glennie, 2020; Ma et al., 2020) based on the promising results from an early study of bathymetry performance capability (Parrish et al., 2019). Additionally, ICESat-2's operational Inland Water Product (ATL13) has been computing along-track bathymetry points at coarse resolution since late 2019 (Jasinski et al., 2020) under favorable cloudiness and water clarity conditions.

Despite these encouraging results, research is needed to develop and quantify the performance of ICESat-2-aided SDB retrievals with the ultimate goal of producing procedures efficient and accurate enough to support global nearshore bathymetric change analysis and worldwide coral reef habitat mapping. This study takes an important first step toward these long-range objectives by developing and testing (both in terms of spatial accuracy and processing times) an operationally efficient end-to-end, and reproducible ICESat-2-aided SDB procedure. To the best of our knowledge, it is the first such study to detail and quantify the accuracy and algorithm efficiency—on a step-by-step basis—of a complete ICESat-2-aided SDB workflow, while simultaneously investigating the achievable accuracies of the resultant bathymetric DEMs using both Sentinel-2 and Landsat 8. The results establish a baseline against which more advanced processing procedures, leveraging machine learning and AI, can be benchmarked. The results also include an analysis of the specific steps that, through further automation or optimization, can best increase end-to-end processing performance. We conclude with a discussion of the current status and next steps toward the long-range goal of enabling repeat bathymetric mapping in coral reef habitats worldwide.

2. Methods and data sources

2.1. Workflow

The workflow for the efficient generation of bathymetric digital elevation models (DEMs) developed and tested in this work is depicted in Figure 1. The inputs consist of ICESat-2 ATL03 (Neumann et al., 2019) geolocated photon returns available in HDF5 file format from nsidc.org and Landsat 8 or Sentinel-2 multispectral imagery available from the U.S. Geological Survey (USGS) Earth Explorer. The output consists of bathymetric DEMs projected in UTM (WGS84(G1762)) with EGM2008 orthometric heights. The spatial resolution of the output models is dependent on the input imagery resolution (30 m Landsat-8 and 10 m Sentinel-2).

The ICESat-2 processing stream starts with the conversion from WGS84 ellipsoid heights to orthometric heights. The importance of this step stems from the fact that that, over even relatively short along-track segment lengths (e.g., a few km), the water surface will generally exhibit a salient tilt when ellipsoid heights are used. The water surface tilt when using ellipsoid heights is attributed to two main components: (1) the geoid gradient (Deng & Featherstone, 2006); and (2) mean dynamic ocean topography (MDT) (Rapp et al., 1994), which has potential to introduce locally large slopes. The mean sea surface gradient, accounting for both
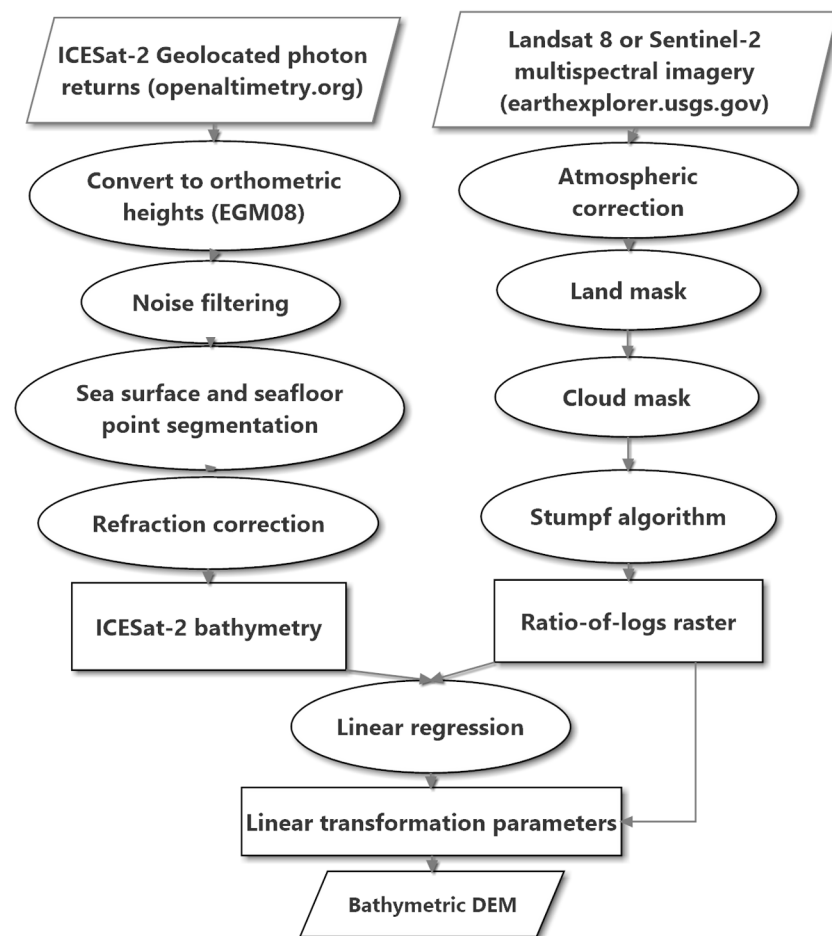
Figure 1. Workflow diagram for procedure developed and tested in this study.

components can reach 10s of cm/km in some areas (Brenner et al., 1990). The noise filtering step is optional, but was found to decrease overall processing times by removing a large number of the water column returns, such that seafloor points can be extracted more efficiently. In this work, the noise filtering was implemented in the form of a simple 2D window operation (with the dimensions being along-track time and elevation), removing points for which the point density within the window is below a user-tunable threshold, which is set based on the background noise rate for the particular beam. A window size of 0.001 s (along track time) by 0.5 m (return photon height) and a default point density threshold of two points per window were found to work well. The seafloor/sea surface point selection step is only semiautomated and consists of generating profile plots of photon returns in MATLAB and using the "Brush/Select Data" tool to manually segment the sea surface and seafloor (bathymetric bottom) points. The seafloor points are then refraction-corrected using the algorithm in Parrish et al. (2019). This algorithm applies a both a planimetric correction and a vertical correction to the coordinates of the ATL03 geolocated photon returns from the seafloor to account for the refraction (bending) and corresponding change in the speed of light at the air-water interface. These corrections are needed, because the ATL03 geolocation procedure was not designed for subaqueous points.

Meanwhile, the multispectral imagery processing stream starts atmospheric correction, which is required for accurate bathymetric retrieval (Caballero & Stumpf, 2020) and performed using the open-source software ACOLITE (Vanhellemont & Ruddick, 2016). Masking out clouds and land reduces computation time and prevents nonwater pixels from impacting the results. The land masking can be greatly aided through the use of existing vector shoreline data (e.g., Sayre et al., 2019), although some level of manual editing is

typically required. The ratio-of-logs algorithm described by Stumpf et al. (2003) and adapted from Caballero et al. (2019) is implemented using these atmospherically corrected blue and green spectral bands:

$$Z_r = \frac{\ln\left(nR_{rs}\left(\lambda_i\right)\right)}{\ln\left(nR_{rs}\left(\lambda_j\right)\right)} \tag{1}$$

The output of equation (1) is a relative (unitless) estimate of bathymetry, based on the ratio of the natural log of the product of the fixed constant n (set to 1,000 in this work, following Stumpf et al., 2003) and the remote sensing reflectance, R_{rs}, of two bands output from ACOLITE. In this case, the blue (center wavelength = 483 nm) and green (center wavelength = 561 nm) bands were used for λ_i and λ_j, respectively. Through pixel-by-pixel application of equation (1), a raster of relative depth estimates is generated, hereafter referred to as the ratio-of-logs image. The ICESat-2 refraction-corrected bathymetric points (a total of 3,539 refraction-corrected points, in this study) are utilized as the SDB seed depths and regressed against the ratio-of-logs DEM pixel values to obtain the parameters of a linear transformation for the final bathymetric data product. More specifically, this involves computing the linear transformation parameters (m_0, m_1) in the equation below (Stumpf et al., 2003):

$$Z_{SDB} = m_1 Z_r + m_0 \tag{2}$$

Finally, equation (2) is applied pixel-by-pixel to create a bathymetric DEM containing EGM2008 seafloor heights for the entire region of interest and with a ground sample distance (GSD) matching that of the input multispectral imagery.

2.2. Site selection

Primary consideration in site selection for this study were: (1) diversity of seafloor type (e.g., sand, coral, seagrass); (2) suitably clear water, since turbidity limits any form of bathymetric lidar, whether airborne or spaceborne (Parrish et al., 2019); (3) availability of cloud-free Landsat 8 and Sentinel-2 data collected close in time to the ICESat-2 data; and (4) the availability of high-accuracy reference data for accuracy assessments of the output bathymetric DEMs. Based on these considerations, the selected study site encompassed the island of St. Croix in the U.S. Virgin Islands (USVI) (Figure 2).

2.3. Data

The ICESat-2 ATL03 geolocated data for two ATLAS beams (GT3R and GT1R) collected from a descending track on December 21, 2018 at approximately 04:40 UTC. The multispectral imagery consisted of Landsat 8 Operational Land Imager (OLI) and Sentinel-2B Multispectral Instrument (MSI) imagery for St. Croix, collected on August 12, 2018 at 14:44 UTC and December 21, 2018 at 14:58 UTC, respectively. The high-resolution airborne bathymetric lidar reference data were collected by NOAA's National Geodetic Survey Remote Sensing Division (NGS/RSD) with a Riegl VQ-820-G from October 12, 2014 to October 26, 2014 and had a stated accuracy of ±0.15 m (1σ). It is important to note that, during the four-year time interval between the acquisition of the airborne bathymetric lidar data and the ICEsat-2, Landsat 8, and Sentinel-2 data collections, the site was impacted by Hurricane Maria (September 20, 2017). Analysis of nearshore seafloor change in this general area conducted by our research group as part of separate studies (Slocum, 2020; Wilson et al., 2019), indicated that the overall level of seafloor elevation change in the nearshore areas of our study site is small enough ($\mu = 11$ cm, $\sigma = 16$ cm, prehurricane versus posthurricane lidar elevation difference in the vicinity of Buck Island) in comparison to typical SDB accuracies that the airborne bathymetric lidar can be used as a suitable reference data set.

3. Results

The goal of this effort is to provide a foundation for SDB that leverages the active bathymetric measurements from ICESat-2 for efficiency of workflow, standardization of approach and performance accuracy. Efficiency of the workflow relative to execution times is provided in Table 1. It is important to note that these times were not based solely on the St. Croix data, but, in fact, are processing time averages for ~10 sites
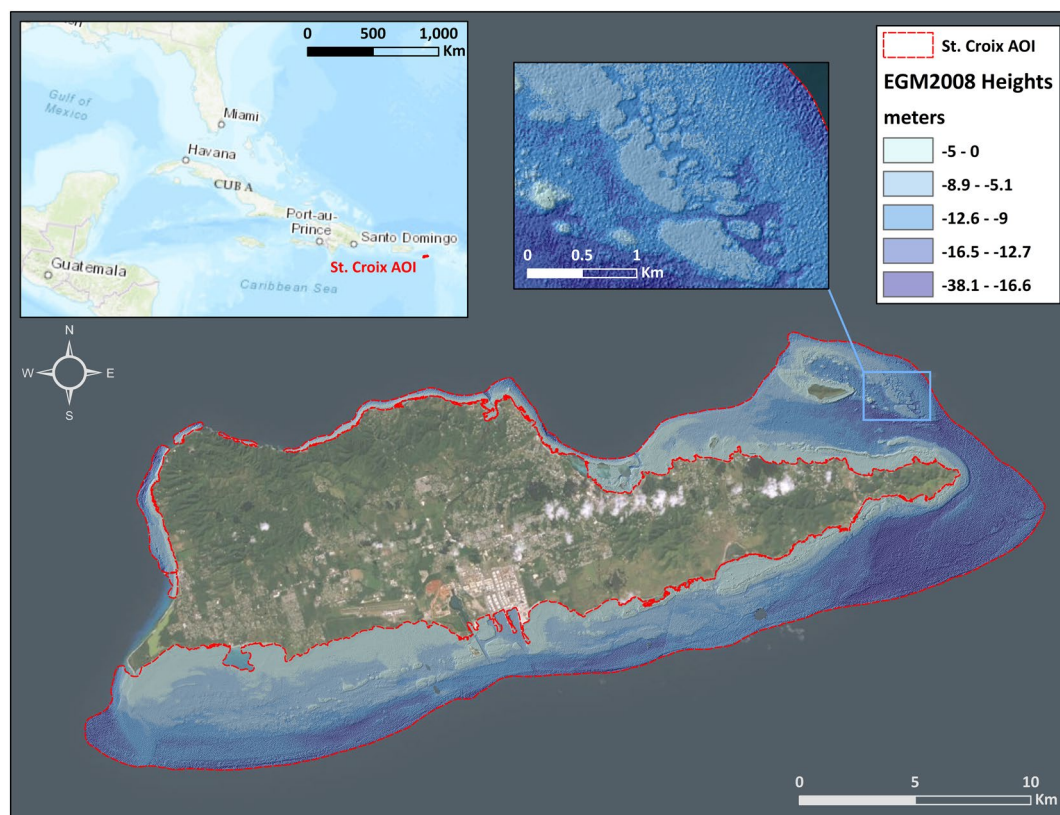
Figure 2. St. Croix, USVI, study site (generated using ArcMap version 10.8.1).

Table 1
Mean Processing Times by Task (Bold) and Subtask (Unbold) Using Both Sentinel-2 and Landsat 8 Imagery

Primary processing step	Subtask	Estimated time	Level of automation
(1) ICESat-2 data extraction		**5 min**	**Semiautomated**
	Noise filtering	<15 s	Automated
	Point classification	5 min/satellite transect	Manual
(2) Refraction correction		**<Negligible>**	**Automated**
(3) Atmospheric correction			**Automated**
	Landsat 8	1 min/6,600 km^2	Automated
	(OR) Sentinel-2	1 min/1,000 km^2	Automated
(4) Ratio of logs creation			**Semiautomated**
	Mask Creation	*1 min/10 km^2	Manual
	Stumpf Algorithm	<2 min	Automated
(5) Final DEM creation		**<10 s**	**Automated**
	Linear regression	*<5 s	Automated
	Application of coefficients/ DEM creation	<5 s	Automated

Note. Asterisks (*) denote steps with higher variability in time, due to the GSD of the input imagery Italicized values are normalized by area since completion time is highly dependent on the total site area. For nonitalicized steps, the time impact of the site area was well within the variability due to other factors, and, therefore, could not be reliably estimated.
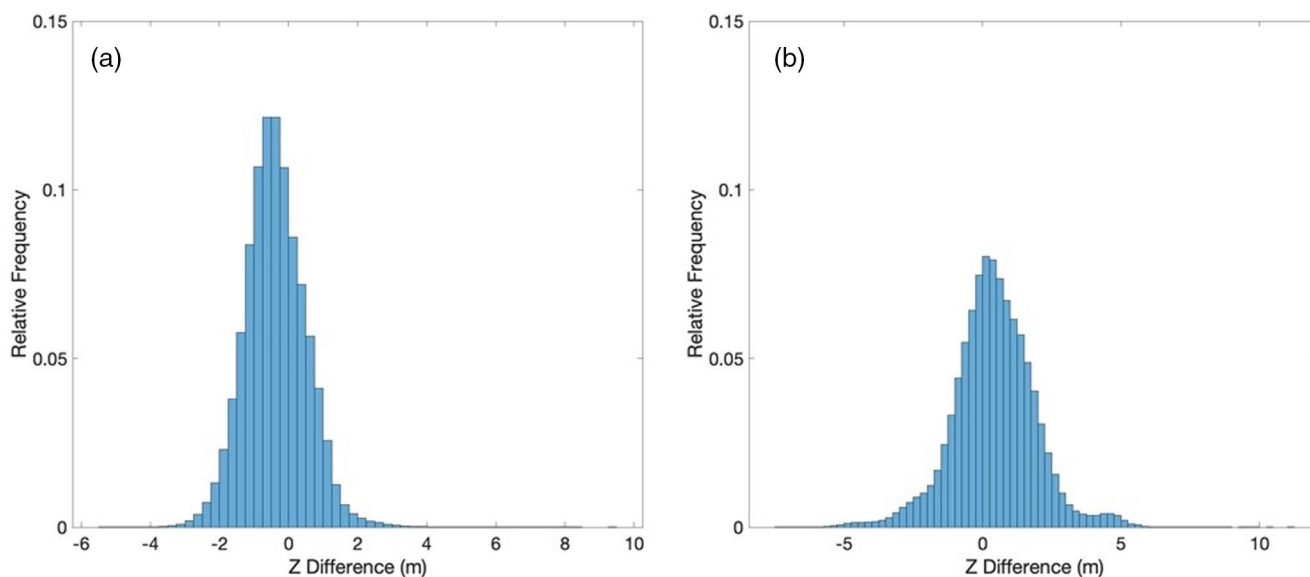
Figure 3. Error distributions from comparisons of ICESat-2-aided SDB against the high-accuracy reference data, when the SDB was generated from Sentinel-2 (A) and Landsat 8 (B). ICESat-2, Ice, Cloud, and land Elevation Satellite-2; SDB, Satellite-Derived Bathymetry.

included in our project webGIS (https://shallowbathymetryeverywhere.com). Total processing times for the selected sites ranged from 17 to 37 min. Although most of the workflow processing steps are automated, the results highlight the need to focus on manual tasks associated with ICESat-2 bathymetry signal extraction and the mask generation for the passive datasets. In this study, the manual steps were completed by an experienced bathymetric lidar analyst.

The bathymetric DEMs for St. Croix produced from the method described were compared against the airborne topobathymetric lidar reference data to assess the accuracy of the SDB models. These airborne lidar points are considered pseudo-GCPs (ground control points) to mimic the established ASPRS bilinear interpolation method for elevation comparisons (Flood, 2004). To accommodate the sheer density of bathymetric bottom classified airborne lidar points, a MATLAB script was written in order to perform random subsampling of the data. These decimated point clouds (which still contained over 1.3 million points each, a value selected to provide both a very large sample size and similar number of points for the two data sets) were then used as spatially distributed pseudo-GCPs for the accuracy assessment of the SDB models. We report the error using two different metrics: Accuracy (z) at the 95% confidence level (as defined by ASPRS, 2004, 2014; FGDC, 1993), and the 95th percentile absolute error. The latter is based on absolute values of the errors, as specified by ASPRS (Flood, 2004) and is more appropriate when the error distribution is non-Gaussian. Error histograms are shown in Figure 3, while summary statistics are provided in Table 2. The R^2 values from the linear regressions of the ICESat-2 refraction-corrected bathymetry on the ratio-of-logs images were 0.94 and 0.92 and for Sentinel-2 and Landsat 8, respectively.

Table 2
Summary Statistics from Accuracy Assessment

	Sentinel-2 SDB	Landsat 8 SDB
Sample size	1,311,297 points	1,320,136 points
Mean	−0.38 m	0.42 m
Minimum	−5.39 m	−7.48 m
Maximum	9.33 m	11.02 m
Standard deviation	0.88 m	1.48 m
Skewness	0.31	−0.01
RMSE	0.96 m	1.54 m
95% Confidence level	1.88 m	3.02 m
95th Percentile	1.86 m	3.13 m

4. Discussion

Several factors may contribute to the accuracy results of the DEM product of the combined SDB and ICESat-2 elevations. It is interesting to note the variability in error statistics between the different zones within the St. Croix study site. The intrasite environmental characteristics were analyzed to determine whether there were clear causes of this variability. Spatially varying turbidity is one possible cause, as the Stumpf algorithm assumes uniform water clarity. This can become especially problematic as the Area of Interest (AOI) size increases, giving rise to potential localized differences in water clarity due to suspended sediment, microalgae,

currents, or other factors. Areas of freshwater (e.g., river) discharge, tidal inlets, and high wave energy may also cause challenges. To assess the spatial variability of water clarity, VIIRS Kd490 plots were assessed. Although the resolution of the VIIRS Kd490 data is rather coarse (750 m GSD), local variability was still noted. For this reason, multiple ICESat-2 transects were incorporated to provide a wider spatial sample as part of the linear regression and explore the water clarity impact on the space-based lidar performance and resultant SDB. The challenge of this approach is actually the variability of the R^2 values across independent ICESat-2 transects and the production of variable transformation coefficients that require some optimal determination across the full AOI through some selective conflation. This is an area that necessitates further investigation. Additionally, although the Stumpf algorithm is somewhat robust to differing substrates or bottom types (through use of the ratio in equation (2), and with the assumption that a uniform brightening or darkening of the seafloor will affect both bands roughly equally), this is another possible contributing factor to the varied results. Through the use of a benthic habitat shapefile mask of St. Croix created by NOAA, at least ten different substrates/cover types represented in varying degrees that intersect with the randomly distributed GCPs were noted. While a transition from one substrate or cover type to another (e.g., sand to seagrass or sand to coral) may have a roughly similar effect on the albedo in the green and blue spectral bands, it is certainly possible that there could be a relative difference in the impact on the two different bands. This would manifest not as a uniform change in intensity (i.e., a uniform brightening or darkening) when transitioning from one substrate to another, but as a change in color.

As of the writing of this paper, the procedures have been applied to 12 separate AOIs to produce bathymetric DEMs. The bathymetric DEMs have been made publicly available in GeoTIFF format via our project webGIS (https://shallowbathymetryeverywhere.com) such that they can be evaluated and used in further studies by other researchers.

Certainly, follow-on studies are warranted as high-resolution imagery could be more rigorously evaluated for the sensitivity of bathymetric error to spatially variable water clarity and substrate. There is also opportunity to pursue additional SDB algorithms within the workflow established in this effort. For the approach presented herein, the Stumpf algorithm itself creates another area of future research—spectral band optimization. These results relied on the typical combination of blue and green spectral bands, but further research could test other possible band combinations in differing water types for geographically optimized SDB products. Regarding automation of the manual portions of the workflow, it is recommended that the two priorities be: (1) cloud and land mask generation, and (2) segmentation of sea surface and seafloor returns. While the second—segmentation—is likely the easier of the two to automate, leveraging advances in machine learning for segmentation tasks, it is the first task—mask generation—that is currently the larger bottleneck. However, additional focus on the segmentation task may result in not only improved efficiency, but also better accuracy, by better defining the specific photon returns within the sea surface and seafloor layers in the point cloud to classify as water surface and seafloor.

5. Conclusions

Global nearshore bathymetry is a high-demand product that is now more readily achievable given NASA's ICESat-2 satellite, the most recent Earth observing laser altimeter poised to provide accurate bathymetric elevation retrievals. These retrievals are important measurements individually but also provide a critical component to SDB using a novel approach for fusion with existing imagery as they provide vertical reference required to produce bathymetric DEMs at the global scale. The fusion workflow presented here for a selected study site creates a baseline for bathymetry generation in SDB accuracy and process efficiency and is poised for future enhancements or analysis and the use of ICESat-2 for bathymetry becomes more mature. To understand the current SDB DEM quality using Landsat 8 and Sentinel-2 imagery the DEMs were compared to an independently derived surface from high-accuracy airborne bathymetric lidar data. Those DEM comparisons for the Sentinel-2 and Landsat-8 analysis indicate RMSE's of 0.96 and 1.54 m, respectively. An important finding was that the Sentinel-2 imagery, with a GSD closest in size to the ICESat-2 footprint (10 m versus 11 m), was found to provide better accuracy than Landsat 8 (30-m GSD). Site-specific variation in environmental characteristics (water clarity, bathymetric relief, etc.) and resolution of the relevant datasets enabled an analysis of the variability in bathymetric DEM accuracy as a function of the type of input imagery. Expanding the analysis to other regions will further inform the impact of environmental

characteristics on the SDB product quality while additional research into SBD conflation techniques and automation will certainly benefit the breadth of the application to benthic studies. A long-range goal of this research is to apply operationally efficient ICESat-2-aided SDB procedures to generate multitemporal bathymetry of coral reef areas around the world, which are experiencing rapid degradation (e.g., Pandolfi et al., 2011). As bathymetric data and derived products, such as seafloor rugosity, have been shown to facilitate benthic reef habitat mapping (e.g., Collings et al., 2019), multitemporal reef bathymetry provided by ICESat-2-aided SDB holds great promise for assessing change and evaluating the efficacy of protection and restoration strategies.

Data Availability Statement

ICESat-2 data are publically available via the National Snow and Ice Data Center (doi: https://doi.org/10.5067/ATLAS/ATL03.003). Landsat 8 is provided via https://doi.org/10.5066/F71835S6 and Sentinel-2 data via https://doi.org/10.5066/F76W992G.

References

Albright, A., & Glennie, C. L. (2020). Nearshore bathymetry for fusion of Sentinel-2 and ICESat-2 observations. *IEEE Geoscience and Remote Sensing Letters*, 1–5. https://doi.org/10.1109/LGRS.2020.2987778

Brenner, A. C., Koblinsky, C. J., & Beckley, B. D. (1990). A preliminary estimate of geoid-induced variations in repeat orbit satellite altimeter observations. *Journal of Geophysical Research*, *95*(C3), 3033–3040.

Caballero, I., & Stumpf, R. P. (2020). Towards routine mapping of shallow bathymetry in environments with variable turbidity: Contribution of Sentinel-2A/B satellites mission. *Remote Sensing*, *12*(3), 451.

Caballero, I., Stumpf, R. P., & Meredith, A. (2019). Preliminary assessment of turbidity and chlorophyll impact on bathymetry derived from Sentinel-2A and Sentinel-3A satellites in South Florida. *Remote Sensing*, *11*(6), 645.

Collings, S., Campbell, N. A., & Keesing, J. K. (2019). Quantifying the discriminatory power of remote sensing technologies for benthic habitat mapping. *International Journal of Remote Sensing*, *40*(7), 2717–2738.

Deng, X., & Featherstone, W. E. (2006). A coastal retracking system for satellite radar altimeter waveforms: Application to ERS-2 around Australia. *Journal of Geophysical Research*, *111*, C06012. https://doi.org/10.1029/2005JC003039

Eugenio, F., Marcello, J., & Martin, J. (2015). High-resolution maps of bathymetry and benthic habitats in shallow-water environments using multispectral remote sensing imagery. *IEEE Transactions on Geoscience and Remote Sensing*, *53*(7), 3539–3549.

Flood, M. (2004). *ASPRS guidelines—Vertical accuracy reporting for Lidar Data*. Available from https://www.asprs.org/a/society/committees/standards/Vertical_Accuracy_Reporting_for_Lidar_Data.pdf

Forfinski-Sarkozi, N. A., & Parrish, C. E. (2016). Analysis of MABEL bathymetry in Keweenaw Bay and implications for ICESat-2 ATLAS. *Remote Sensing*, *8*, 772.

Jasinski, M., Stoll, J., Cook, W., Ondrusek, M., Stengel, E., & Brunt, K. (2016). Inland and near-shore water profiles derived from the high-altitude Multiple Altimeter Beam Experimental Lidar (MABEL). *Journal of Coastal Research*, *76*(1), 44–55.

Jasinski, M., Stoll, J., Hancock, D., Robbins, J., Nattala, J., Pavelsky, T., et al. (2020). *"Algorithm theoretical basis document (ATBD) for inland water data products, ATL13, Version 3," Release Date March 1, 2020*. (pp. 112). Greenbelt, MD: NASA Goddard Space Flight Center. Retrieved from https://doi.org/10.5067/L870NVUK02YA

Jerlov, N. G. (Ed.). (1976). *Marine optics*. Amsterdam: Elsevier.

Ma, Y., Xu, N., Liu, Z., Yang, B., Yang, F., Wang, X.H., & Li, S. (2020). Satellite-derived bathymetry using the ICESat-2 lidar and Sentinel-2 imagery datasets. *Remote Sensing of Environment*, *250*, 112047.

Magruder, L., Brunt, K., & Alonzo, M. (2020). Horizontal geolocation validation for ICESat-2 with corner-cube retroreflectors. *Remote Sensing*, *12*(21), 3653. https://doi.org/10.3390/rs/12213653

Magruder, L., Neumann, T. A., Brunt, K., Farrell, S., Fricker, H., Gardner, A., et al. (2019). New Earth orbiter provides a sharper look at a changing planet. *Eos, Transactions American Geophysical Union*, *100*. https://doi.org/10.1029/2019EO133233

Markus, T., Neumann, T., Martino, A., Abdalati, W., Brunt, K., Csatho, B., et al. (2017). The Ice, Cloud, and land Elevation Satellite-2 (ICESat-2): Science requirements, concept, and implementation. *Remote Sensing of Envirnoment*, *190*, 260–273. https://doi.org/10.1016/j.rse.2016.12.029

Mavraeidopoulos, A. K., Pallikaris, A., & Oikonomou, E. (2017). Satellite derived bathymetry (SDB) and safety of navigation. *The International Hydrographic Review*, *17*, 7–19.

Neumann, T. A., Brenner, A., Hancock, D., Robbins, J., Saba, J., Harbeck, K., et al. (2020). ATLAS/ICESat-2 L2A Global Geolocated Photon Data, Version 3. Boulder, CO: NASA National Snow and Ice Data Center Distributed Active Archive Center. Retrieved from https://doi.org/10.5067/ATLAS/ATL03.003

Neumann, T. A., Martino, A. J., Markus, T., Baeb, S., Bock, M. R., Brenner, A. C., et al. (2019). The Ice, Cloud and Land Elevation Satellite-2 mission: A global geolocated photon product derived from the Advanced Topographic Laser Altimeter System. *Remote Sensing of Environment*, *233*, 111325. https://doi.org/10.1016/j.rse.2019.111325

Pandolfi, J. M., Connolly, S. R., Marshall, D. J., & Cohen, A. L. (2011). Projecting coral reef futures under global warming and ocean acidification. *Science*, *333*(6041), 418–422.

Parrish, C. E., Magruder, L. A., Neuenschwander, A. L., Forfinski-Sarkozi, N., Alonzo, M., & Jasinski, M. (2019). "Validation of ICESat-2 ATLAS bathymetry and analysis of ATLAS's bathymetric mapping performance. *Remote Sensing*, *11*(14), 1634.

Pe'eri, S., Madore, B., Nyberg, J., Snyder, L., Parrish, C., & Smith, S. (2016). Identifying bathymetric differences over Alaska's North Slope using a satellite-derived bathymetry multi-temporal approach. *Journal of Coastal Research*, *76*(76), 56–63.

Pittman, S., & Monaco, M. E. (2008). *Fish assemblages and benthic habitats of Buck Island Reef National Monument (St. Croix, U.S. Virgin Islands) and the surrounding seascape: A characterization of spatial and temporal patterns* (NOAA Tech. Memo. NOS NCCOS 71). National Centers for Coastal Ocean Science (U.S.).

Poursanidis, D., Traganos, D., Reinartz, P., & Chrysoulakis, N. (2019). On the use of Sentinel-2 for coastal habitat mapping and satellite-derived bathymetry estimation using downscaled coastal aerosol band. *International Journal of Applied Earth Observation and Geoinformation*, *80*, 58–70.

Rapp, R. H., Yi, Y., & Wang, Y. M. (1994). Mean sea surface and geoid gradient comparisons with TOPEX altimeter data. *Journal of Geophysical Research*, *99*(C12), 24657–24667.

Sayre, R., Noble, S., Hamann, S., Smith, R., Wright, D., Breyer, S., et al. (2019). A new 30 meter resolution global shoreline vector and associated global islands database for the development of standardized ecological coastal units. *Journal of Operational Oceanography*, *12*(Suppl 2), S47–S56.

Slocum, R .K. (2020). *New simulation and fusion techniques for assessing and enhancing UAS topographic and bathymetric point cloud accuracy* (PhD dissertation). Corvallis, OR:Oregon State University.

Stumpf, R. P., Holderied, K., & Sinclair, M. (2003). Determination of water depth with high-resolution satellite imagery over variable bottom types. *Limnology and Oceanography*, *48*(1 Part 2), 547–556.

Vanhellemont, Q., & Ruddick, K. (2016). ACOLITE processing for Sentinel-2 and Landsat-8: Atmospheric correction and aquatic applications. In *Ocean Optics Conference Proceedings* (p. 12), Victoria, BC, Canada.

Wilson, N., Parrish, C. E., Battista, T., Wright, C. W., Costa, B., Slocum, R. K., et al. (2019). *Mapping seafloor relative reflectance and assessing coral reef morphology with EAARL-B topobathymetric Lidar waveforms*. Estuaries and Coasts, 1–15. https://doi.org/10.1007/s12237-019-00652-9